3D positional metrology of a virus-like nanoparticle with topologically structured light

Yu Wang [1], Eng Aik Chan [2], Carolina Rendón-Barraza [2], Yijie Shen [2], Eric Plum [1], Kevin F. MacDonald [1], Jun-Yu Ou [3*] and Nikolay I. Zheludev [1, 2]

1. Optoelectronics Research Centre and Centre for Photonic Metamaterials, University of Southampton, Southampton, UK
2. Centre for Disruptive Photonic Technologies, TPI & SPMS Nanyang Technological University, Singapore
3. School of Physics and Astronomy, University of Southampton, Southampton, UK

*bruce.ou@soton.ac.uk

Abstract: Locating and identifying viruses in *in-vitro* optical measurements is desirable for disease control; however, the sub-diffraction-limit dimensions and low refractive index contrast of viruses make this challenging. Here, we introduce a 3D positional nanometrology for a virus-like 100 nm polystyrene sphere, that can reveal the position of the nanoparticle with deeply sub-wavelength accuracy using topologically structured light illumination and machine learning. Scattering of topologically structured light is highly sensitive to the position of a nano-object. Exploiting this, our experiments demonstrate deeply sub-wavelength (λ) precision reaching 5 nm (λ/91). Our findings indicate a route towards label-free *in-vitro* nanometrology of viruses and similar nano-objects with precision far beyond the Abbe-Rayleigh diffraction limit.

In optical nanoimaging and metrology applications, the acquisition of accurate object information—morphology, size, and position—beyond the Abbe-Rayleigh diffraction limit of conventional microscopy remains a long-standing barrier to overcome. In the last ten years, there has been a remarkable enhancement in the spatial resolution of far-field optical imaging and metrology, surpassing the conventional ~λ/2 limit, where λ represents the wavelength of light. Today, a multitude of advanced techniques, including fluorescent and structured-illumination-based methodologies, both deterministic and stochastic, as well as single-molecule localization microscopies, have become standard in biological imaging. These techniques consistently achieve resolutions of a few tens of nanometers, or better than λ/10 [1-4]. One of the most challenging tasks in bioimaging is to observe viruses since they are small and have low refractive index contrast with their surroundings to be seen in a conventional optical microscope. Viruses can be imaged with atomic-force microscopy (AFM) and cryo-electron microscopy (cryo-EM), but AFM is slow and invasive while cryo-EM is invasive and only reconstructs samples in matrices at low temperatures [5-7]. The localization of viruses is crucial for disease control: How a virus settles and persists on surfaces of different types of materials is key information for the development of disease control strategies and monitoring of anti-microbial agents [8].

Topologically structured light fields, in particular super-oscillatory illumination, generated through multi-wave interference by purposely designed intensity and phase masks, can contain highly localized intensity hotspots, phase singularities, zones of energy backflow and high phase gradients at dimensional scales orders of magnitude smaller than the wavelength of light [9-11]. Recently such fields have resolved the position of a macroscopic object—a nanowire—with subatomic precision [12]. Such super-oscillatory illumination fields also have been used in label-free biological tissue and nanoparticle imaging applications [9-11], where the resolution improvement does not depend on the intensity of the illuminating laser in contrast to luminescence-based techniques, meaning that living cells can be imaged in real-time with minimal perturbation. Such investigations suggest that interaction with rapid spatial variations of topological fields will enable *in-vitro* metrology of viruses at the nanometer scale.

In recent years, artificial intelligence and deep learning have shown superiority over some task-specific algorithms in various applications. More specifically, deep learning based on artificial neural network training has considerably improved precision in image segmentation [13-15], face recognition [16-18], object detection [19, 20], and dimension prediction [21, 22].

Here, we show that topological light fields—specifically super-oscillatory fields—can be used to precisely measure the three-dimensional position of a subwavelength dielectric nanoparticle, with a similar size and refractive index of a typical influenza virus [23], achieved by a deep learning-enabled analysis of the particle's scattering intensity patterns. We demonstrate nanometer-level positional measurement precision, which reaches λ/91 and significantly exceeds the diffraction limit (~λ/2).

The principle of the proposed nanometrology scheme is shown in Fig. 1, where a pair of spatial light modulators [24, 25] is used to create a topologically structured super-oscillatory field (Fig. 1a, d), enabling us to control, optimize the hotspot, and scan across the nanoparticle. The phase profile of such a field (Fig. 1a) has singularities (indicated by circles) which can interact with a virus-like nanoparticle (drawn as a gray virus) resulting in changes of the transmission scattering pattern. A deep learning process with a neural network trained on a-priori known positions of a nanoparticle is used to analyze scattering patterns for the determination of unknown positions of the nanoparticle.

We demonstrate, both in experiments and simulations, 3D positional measurements for a 100 nm spherical polystyrene particle—resembling, by size and refractive index, an influenza virus [23]. The sample is prepared by drop-casting polystyrene particles with a diameter of 100 nm onto a glass substrate. An isolated particle is then located by scanning electron microscopy, as shown in Fig. 1c. We utilize a pair of spatial light modulators (Meadowlark P512) to convert the Gaussian, y-polarized input laser beam at wavelength $\lambda = 488$ nm into the balanced superposition of two circular prolate spheroidal wavefunctions (S1 and S2) to achieve a super-oscillatory hotspot ($E(r/\lambda) = 0.1206$ S1 (r/λ) + S2 (r/λ), where r is radial distance from the beam axis, following references [9, 26]) with a field of view of λ and a full width at half maximum of 0.42λ, as shown in Fig. 1d. The experimental setup is illustrated in Fig. 1b, where the virus-like nanoparticle is illuminated by the super-oscillatory light and the scattered light is collected in transmission via a pair of 100×, NA = 0.9 microscope objectives (L1 and L2). The nanoparticle sample mounted on a piezoelectric translation stage is scanned relative to the super-oscillatory hotspot over a 400 (~0.82λ) × 400 × 400 nm^3 volume with an interval of 20 nm, acquiring 9261 diffraction images with a 16-bit camera at the height of 1.6 μm relative to the hotspot plane.

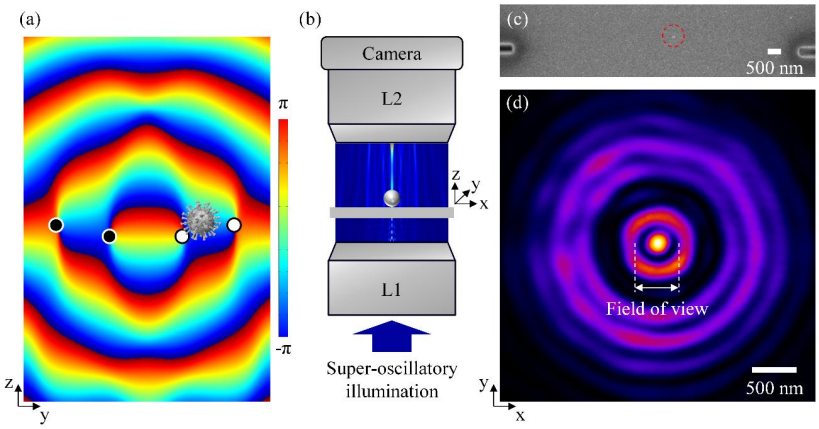

Fig. 1: (a) The cross-sectional phase profile ($\varphi(E_y)$) of a super-oscillatory, topologically structured, coherent optical field. Singularities are indicated by circles (black/white for anticlockwise increasing/decreasing phase). A virus particle depiction, to scale, is overlaid. (b) Experimental setup schematic for positional nanometrology as reported here. The virus-like nanoparticle is illuminated by super-oscillatory light, and its diffraction pattern is recorded at the distance of 1.6 μm from the plane of the super-oscillatory hotspot. (c) SEM of a virus-like nanoparticle with a diameter of 100 nm indicated by a red dotted circle. (d) Super-oscillatory intensity distribution in the plane of the super-oscillatory hotspot.

Deep learning, based on linear regression followed by nonlinear activation functions, uses a hierarchy of training layers between the input and the output. Each training layer transforms the output of the previous layer into more abstract representations which are ultimately aggregated in the output layer to achieve the prediction. In general, learning more complex features requires more layers. However, the training accuracy saturates and then degrades rapidly with increasing depth in plain networks [27, 28]. To avoid such a problem, we adopt a deep residual network, with the advantages of easier optimization and considerably more accuracy from deeper layers, in training and predicting the 3D positions of the nanoparticle from scattering patterns. The approach involves explicitly redefining the layers as learning residual functions based on the layer inputs, rather than learning functions without any references [27, 28].

Here, we use a 34-layer residual network (ResNet34), with the same architecture as in reference [27]. The first convolutional layer is a 7×7 kernel convolutional layer with 64 output channels with a stride of 2 followed by a 3×3 max pooling layer with a stride of 2. It is further structured into 4 stages with different numbers of residual blocks – specifically 3, 4, 6, and 3 blocks, sequentially. Within these stages, each block contains multiple residual units, and each unit consists of 3 convolutional layers, culminating in an identity connection (shortcut connection) that bypasses one or more layers, helping preserve information flow and alleviating the vanishing gradient problem. The activation function employed throughout the network is the rectified linear unit (ReLU), except for the final operation within each block. The learned features on the final residual layer are extracted by an average pooling layer, followed by a 512 fully connected layer and 3 output neurons layer, where the output neurons retrieve the x, y and z coordinates of the nanoparticle respectively. The network is trained using the Adam stochastic optimization method [29], and the neural network is optimized by minimizing the mean absolute error loss function.

From the full library of 9261 diffraction images of a virus-like nanoparticle, 7408 images (80%) are selected at random for the training of the neural network, 926 (10%) images as the validation dataset, and 927 (10%) images for testing—i.e., retrieving unknown 3D positions of the nanoparticle via the pre-trained network. After completion of the training using 7408 scattering patterns of the nanoparticle with a-priori known positions, the network is ready for predicting the unknown 3D positions. To learn the data without overfitting and guided by the training and validation loss, we repeat the training process 500 times, using a random training order of images with each time.

To illustrate the significance of the super-oscillatory field in such optical metrology, we compare the measuring error under two different illuminations, i.e., super-oscillatory and tightly focused Gaussian illuminations. Figure 2 demonstrates the discrepancy between optically measured and ground-truth positions of the nanoparticle in experiments with super-oscillatory illumination (Fig. 2a) and tightly focused Gaussian illumination (Fig. 2b). Here, 927 measurements are completed, and each dot represents the 3D absolute error between predicted and actual position for one testing measurement, calculated by:

$$\Delta_i = |R_i - T_i| \tag{1}$$

where i is x, y, or z. R_i denotes the retrieved 3D coordinate value offered by the neural network and T_i is the true position of the nanoparticle. In the experiment, the displacement of the piezoelectric stage loaded with the sample is used to record the true position of the nanoparticle. The input for the neural network is the scattered light pattern collected by the camera with a field of view of 6.3 μm and 12.6 nm effective pixel size. To quantify the precision of this optical metrology, we calculate the standard deviation σ_i between retrieved and actual positions according to:

$$\sigma_i = \sqrt{\frac{\sum_{j=1}^{j=927}(\Delta_i)^2}{927}} \tag{2}$$

where i is x, y, or z and j refers to measurements from the 1st to the 927th. With super-oscillatory illumination, we experimentally achieve measurement standard deviations of 7.4 nm (λ/66) and 5.3 nm (λ/91) in the x and y directions respectively, and 17.6 nm (λ/28) in the light propagating direction z (Fig. 2a). That measuring precision in the x-y plane is superior to that in the light propagating direction is attributed to larger mechanical noise of the piezoelectric translation stage due to environmental instability in the light propagation direction than in the lateral directions.

In addition to the assistance of the neural network, the precision of positional measurement of the nanoparticle indeed benefits from the introduction of topologically structured light. Here, using the same nanoparticle, we also experimentally compare to the case of Gaussian illumination with the same wavelength and a full width at half maximum of λ (same size as the field of view of the hotspot in the case of the super-oscillatory illumination), shown in Fig. 2b. In all directions, the measurement precision is inferior to that with super-oscillatory illumination. For Gaussian illumination, the standard deviations are 24.9 nm (λ/20), 10.2 nm (λ/48), and 45.2 nm (λ/11) along the x, y, and z-axis respectively. In conclusion, our results indicate that the interaction of a sub-wavelength-size particle with rapid spatial variations of topologically structured light pushes positional nanometrology further beyond the diffraction limit.

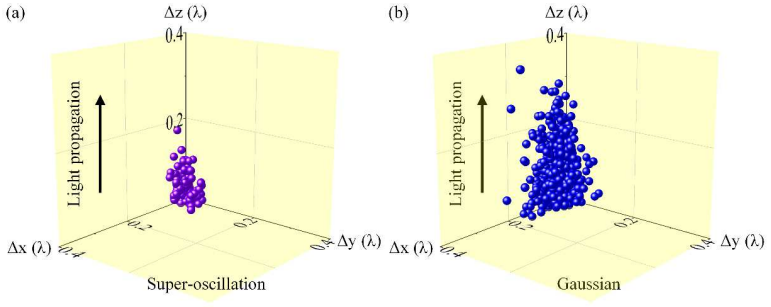

Fig. 2: Absolute errors of 3D positions of the virus-like nanoparticle measured with (a) super-oscillatory and (b) Gaussian illumination. Each dot indicates the absolute difference between the predicted and ground-truth positions of the nanoparticle. The incident light propagates along the z-axis.

For optical metrology as presented here, a sufficient field of view of the diffraction images is essential to include the necessary information concerning the object under assessment, playing a critical role in ensuring measuring precision. However, images with a large field of view necessitate the use of high-performance camera for image capture and substantial computational resources for neural network training. In metrology methods, utilizing images with a restricted field of view frequently results in compromised precision. Figure 3 shows the dependence of metrological precision on the field of view of training images in our setup, where there is a gradual enhancement in measuring precision (i.e., σ_x, σ_y, and σ_z from 0.0574λ, 0.0301λ, and 0.1155λ to 0.0152λ, 0.0109λ, and 0.0362λ) as the field of view of images expands from 1.26 μm to 6.3 μm (i.e., from left to right). Notably, even training images with the smallest field of view of only 1.26 μm are sufficient to achieve 0.1155λ positional measuring precision, which is still far beyond the Abbe–Rayleigh diffraction limit.

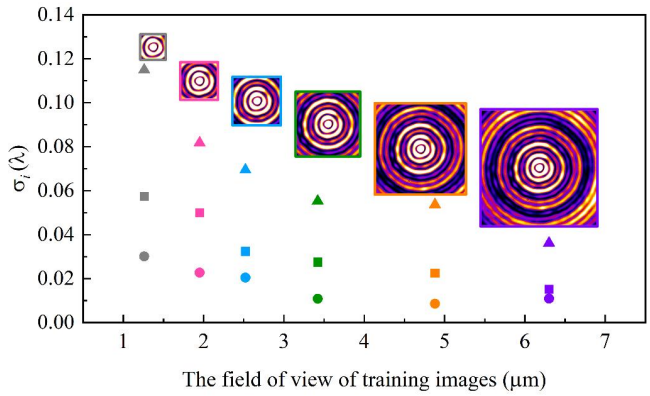

Fig. 3: Dependence of metrological precision on the field of view of training images, where the squares, dots, and triangles denote the positional measuring precision in the x, y, and z directions respectively.

To explore the limits of achievable precision and to gain insight into experimental limitations discussed above, we conduct numerical modelling, which avoids any mechanical drift and environmental instability and mimics the experiment under a number of idealized assumptions. We acquire 9261 numerical diffraction images with the same 6.3 μm field of view as in the experiment and subsequently split them at random as training (7408 images, 80%), validation (926 images, 10%), and testing (927 images, 10%) datasets for the same neural network processing. After training with the computed intensity patterns scattered by the polystyrene particle, the above constructed neural network was ready to retrieve unknown positional information about this particle. As demonstrated in Fig. 4b, the retrieved precisions in all three directions in the simulation are significantly improved compared with the experimental results, the standard deviations are 6.4 nm (λ/76), 4.9 nm (λ/100), and 1.5 nm

(λ/325) along the x, y, and z-axis respectively. Our simulations indicate that a hypothetical ideal experiment that is not affected by environmental effects and instabilities could achieve a considerable improvement of measuring precision compared to our experiment. In particular, they indicate that positional measurements in the light propagation direction with a precision that is at least as good as for measurements of lateral positions should be possible.

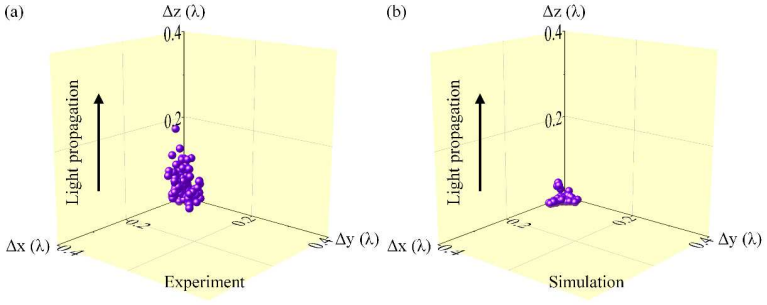

Fig. 4: Absolute errors of positions of the virus-like nanoparticle, achieved by training scattered images of super-oscillatory light collected in (a) experiment and (b) numerical modelling.

In summary, we have demonstrated 3D positional nanometrology with a deeply sub-wavelength precision which uses a neural network to retrieve the position of a virus-like particle from its scattering intensity patterns upon topological illumination. This technique can locate the virus-like nanoparticle within milliseconds, which is determined by the exposure time of a single image taken by a camera. Importantly, it has no requirement of fluorescent labelling thus avoiding photodamage effects. We see potential applications in *in-vitro* imaging, metrology, and tracing of viruses and nano-objects.

Research funding: This work is supported by the UK Engineering and Physical Science Research Council (grants EP/T02643X/1) and the Singapore Ministry of Education (grant MOE2016-T3-1-006).

Author contribution: Yu Wang and Jun-Yu Ou conceived, planned and carried out the experiments. Yu Wang planned and carried out the simulations. Eng Aik Chan constructed the neural network. Carolina Rendón-Barraza prepared the sample. Yu Wang took the lead in writing the manuscript. Eric Plum, Kevin F. MacDonald, Jun-Yu Ou and Nikolay I. Zheludev supervised the work and contributed to the interpretation of the results. All authors provided critical feedback and helped shape the research, analysis and manuscript.

Conflict of interest: The authors declare no conflict of interest.

Data availability statement: The data that support the findings of this study are openly available in the University of Southampton ePrints research repository at https://doi.org/10.5258/SOTON/xxxxx.

References

(1) Xu, J.; Tehrani, K. F.; Kner, P. Multicolor 3D super-resolution imaging by quantum dot stochastic optical reconstruction microscopy. *ACS nano* **2015**, *9* (3), 2917-2925.
(2) Bates, M.; Huang, B.; Dempsey, G. T.; Zhuang, X. Multicolor super-resolution imaging with photo-switchable fluorescent probes. *Science* **2007**, *317* (5845), 1749-1753.
(3) Willig, K. I.; Rizzoli, S. O.; Westphal, V.; Jahn, R.; Hell, S. W. STED microscopy reveals that synaptotagmin remains clustered after synaptic vesicle exocytosis. *Nature* **2006**, *440* (7086), 935-939.
(4) Rust, M. J.; Bates, M.; Zhuang, X. Sub-diffraction-limit imaging by stochastic optical reconstruction microscopy (STORM). *Nat Methods* **2006**, *3* (10), 793-795. DOI: 10.1038/nmeth929.
(5) Zhang, R.; Hryc, C. F.; Cong, Y.; Liu, X.; Jakana, J.; Gorchakov, R.; Baker, M. L.; Weaver, S. C.; Chiu, W. 4.4 Å cryo-EM structure of an enveloped alphavirus Venezuelan equine encephalitis virus. *The EMBO journal* **2011**, *30* (18), 3854-3863.
(6) de Pablo, P. J. Atomic force microscopy of virus shells. In *Seminars in Cell & Developmental Biology*, 2018; Elsevier: Vol. 73, pp 199-208.

(7) Bao, K.; Qi, X.; Li, Y.; Gong, M.; Wang, X.; Zhu, P. Cryo-EM structures of infectious bursal disease viruses with different virulences provide insights into their assembly and invasion. *Science Bulletin* **2022**, *67* (6), 646-654.
(8) Aboubakr, H. A.; Sharafeldin, T. A.; Goyal, S. M. Stability of SARS-CoV-2 and other coronaviruses in the environment and on common touch surfaces and the influence of climatic conditions: a review. *Transboundary and emerging diseases* **2021**, *68* (2), 296-312.
(9) Rogers, E. T.; Quraishe, S.; Rogers, K. S.; Newman, T. A.; Smith, P. J.; Zheludev, N. I. Far-field unlabeled super-resolution imaging with superoscillatory illumination. *Apl Photonics* **2020**, *5* (6), 066107.
(10) Zheludev, N. I.; Yuan, G. Optical superoscillation technologies beyond the diffraction limit. *Nature Reviews Physics* **2022**, *4* (1), 16-32.
(11) Kozawa, Y.; Matsunaga, D.; Sato, S. Superresolution imaging via superoscillation focusing of a radially polarized beam. *Optica* **2018**, *5* (2), 86-92.
(12) Liu, T.; Chi, C.-H.; Ou, J.-Y.; Xu, J.; Chan, E. A.; MacDonald, K. F.; Zheludev, N. I. Picophotonic localization metrology beyond thermal fluctuations. *Nature Materials* **2023**, 1-4.
(13) Ke, R.; Bugeau, A.; Papadakis, N.; Kirkland, M.; Schuetz, P.; Schönlieb, C.-B. Multi-task deep learning for image segmentation using recursive approximation tasks. *IEEE Transactions on Image Processing* **2021**, *30*, 3555-3567.
(14) Liu, X.; Song, L.; Liu, S.; Zhang, Y. A review of deep-learning-based medical image segmentation methods. *Sustainability* **2021**, *13* (3), 1224.
(15) Ghosh, S.; Das, N.; Das, I.; Maulik, U. Understanding deep learning techniques for image segmentation. *ACM Computing Surveys (CSUR)* **2019**, *52* (4), 1-35.
(16) Schroff, F.; Kalenichenko, D.; Philbin, J. Facenet: A unified embedding for face recognition and clustering. In *Proceedings of the IEEE conference on computer vision and pattern recognition*, 2015; pp 815-823.
(17) Arsenovic, M.; Sladojevic, S.; Anderla, A.; Stefanovic, D. FaceTime—Deep learning based face recognition attendance system. In *2017 IEEE 15th International symposium on intelligent systems and informatics (SISY)*, 2017; IEEE: pp 000053-000058.
(18) Wang, H.; Guo, L. Research on face recognition based on deep learning. In *2021 3rd International Conference on Artificial Intelligence and Advanced Manufacture (AIAM)*, 2021; IEEE: pp 540-546.
(19) Zhao, Z.-Q.; Zheng, P.; Xu, S.-t.; Wu, X. Object detection with deep learning: A review. *IEEE transactions on neural networks and learning systems* **2019**, *30* (11), 3212-3232.
(20) Moon, J.; Lim, S.; Lee, H.; Yu, S.; Lee, K.-B. Smart Count System Based on Object Detection Using Deep Learning. *Remote Sensing* **2022**, *14* (15), 3761.
(21) Rendón-Barraza, C.; Chan, E. A.; Yuan, G.; Adamo, G.; Pu, T.; Zheludev, N. I. Deeply sub-wavelength non-contact optical metrology of sub-wavelength objects. *APL Photonics* **2021**, *6* (6). DOI: 10.1063/5.0048139.
(22) Pu, T.; Ou, J. Y.; Papasimakis, N.; Zheludev, N. I. Label-free deeply subwavelength optical microscopy. *Applied Physics Letters* **2020**, *116* (13). DOI: 10.1063/5.0003330.
(23) Kang, P.; Schein, P.; Serey, X.; O'Dell, D.; Erickson, D. Nanophotonic detection of freely interacting molecules on a single influenza virus. *Scientific Reports* **2015**, *5* (1), 12087.
(24) Yang, H.; Lin, E. Y.; Kutulakos, K. N.; Eleftheriades, G. V. Sub-wavelength passive single-shot computational super-oscillatory imaging. *Optica* **2022**, *9* (12), 1444-1447.
(25) Pu, T.; Ou, J. Y.; Savinov, V.; Yuan, G.; Papasimakis, N.; Zheludev, N. I. Unlabeled Far-Field Deeply Subwavelength Topological Microscopy (DSTM). *Adv Sci (Weinh)* **2020**, *8* (1), 2002886. DOI: 10.1002/advs.202002886.
(26) Rogers, K. S.; Bourdakos, K. N.; Yuan, G. H.; Mahajan, S.; Rogers, E. T. Optimising superoscillatory spots for far-field super-resolution imaging. *Optics Express* **2018**, *26* (7), 8095-8112.
(27) He, K.; Zhang, X.; Ren, S.; Sun, J. Deep residual learning for image recognition. In *Proceedings of the IEEE conference on computer vision and pattern recognition*, 2016; pp 770-778.
(28) Zhang, Y.; Tian, Y.; Kong, Y.; Zhong, B.; Fu, Y. Residual dense network for image super-resolution. In *Proceedings of the IEEE conference on computer vision and pattern recognition*, 2018; pp 2472-2481.
(29) Jais, I. K. M.; Ismail, A. R.; Nisa, S. Q. Adam optimization algorithm for wide and deep neural network. *Knowledge Engineering and Data Science* **2019**, *2* (1), 41-46.